

EFFECTS OF THE DIFFERENT LASER BEAM PROFILES ON THE TUNNELING IONIZATION WITH COULOMB CORRECTION INCLUDED

TATJANA B. MILADINOVIC¹, MIRKO M. RADULOVIC², JASNA M. STEVANOVIC²

¹ Institute for Information Technologies, University of Kragujevac,
Jovana Cvijića bb, 34000 Kragujevac, Serbia

E-mail: tanja.miladinovic@uni.kg.ac.rs

² Faculty of Science, University of Kragujevac, Radoja Domanovića 12,
34000 Kragujevac, Serbia

E-mail: mirko.radulovic@pmf.kg.ac.rs

E-mail: jasna.stevanovic@pmf.kg.ac.rs

Received April 1, 2022

Abstract. The aim of this paper was to theoretically investigate the applicability of lasers with 10.6 mm and 800 nm wavelength and different spatial distributions on tunneling ionization of alkali atoms. It includes a comparative study of ionization rate with two expressions for initial non-zero momentum of ejected electron. Results show that ionization rates for non-phased and LG(0,1)* spiral-phased linearly polarized laser beams are sensitive to the type of laser, cause different exit points, reach maxima on different intensity values, and have the dissimilar manner of decrease.

Key words: tunneling ionization, Coulomb correction, LG(0,1)* spiral-phase laser beam.

1. INTRODUCTION

For more than sixty years the non-linear processes of atom ionization by laser electromagnetic field have been investigated both in its experimental and theoretical aspects. Up to now, many efforts have been made to analyze and to understand these processes [1–3]. In his seminal paper [4] Keldysh described the interaction in the dipole, single-active-electron (SAE) approximation, using strong-field approximation (SFA): before the ionization process, the active electron is considered unperturbed by the laser field and, therefore, it interacts only with the atomic potential; after the ionization process, the ejected electron is considered as a free particle propagating only in the presence of the external electromagnetic field and its interaction with the residual atomic core is neglected.

Keldysh also showed that, based on the value of the parameter $\gamma = \omega\sqrt{2E_i}/F$ (here given in the atomic units system: $e = m_e = \hbar = 1$, used throughout this paper), where E_i is ionization potential of atom in question, ω is the frequency, and F is the strength of the applied laser field, these processes have two extremes: multiphoton

ionization processes, $\gamma > 1$ (when weak almost static electric field cannot significantly influence the atom potential) and tunneling ionization processes, $\gamma \ll 1$ (in this case the almost static laser field is so strong that it deforms the atom potential creating the barrier through which the electron can tunnel). As the intensity increases, the length of the barrier that electrons must pass through decreases and the electrons can leave the atom in the manner forbidden classically. In this case, and based on Landau-Dykhne approximation, the ionization rate is given as $w_{if} = \exp[-2(2E_i)^{3/2}/3F]$.

Among the main theoretical approaches used in strong field laser atom physics two are especially distinguished: Perelomov, Popov and Terent'ev (PPT) and Ammosov, Delone and Krainov (ADK). Perelomov *et al.* applied the semiclassical approach which allowed to account for the effects of Coulomb potential in the calculation process, thus developing the method for determining the atom ionization rate in an alternating laser field [5]. Two decades later, Ammosov *et al.* managed to extend the PPT result to complex atoms and ions [6]; their model is now known as ADK theory and is still widely used in the theoretical interpretation of many ionization experiments [7, 8].

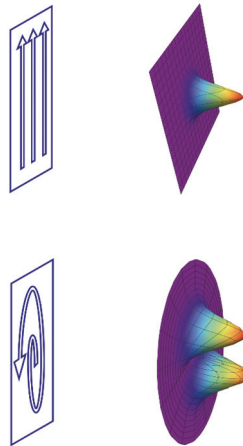


Fig. 1 – The laser beam profile in two modes, linear and spiral [19].

The process of tunneling ionization of electrons when an atom is exposed to a strong laser field of linear, circular, or elliptical polarization already has been described and investigated in numerous papers [9–12]. Also, the ionization rate is maximal for zero initial momentum of ejected electron, but a new information about the ionization processes can be obtained when the initial momentum of electron is different from zero [13]. After that, the extensive research about influence of non-zero initial momentum of ejected electron was investigated in numerous papers [14, 15] but only for linear and circularly polarized laser beams. That is the reason why in this paper is examined how ionization process will unfold when the laser beam is a radially polarized,

concretely when polarization has a Laguerre-Gaussian (LG) ring intensity distribution, with radial index 0 and azimuthal index 1. Radially polarized LG(0,1)* mode is a linear combination of the x -polarized LG(0,1) and y -polarized LG(1,0) [16]. Spiral phase mode is special form of LG(0,1)* radially polarized beam which is obtained using SPE (spiral phase element) [17, 18]. Because the LG(0,1)* spiral-phase mode can appear in all states of polarization, be it linear, circular, or elliptical, in this paper we chose that beam passes through the linear polarizer [19], and laser field intensities lie within the range of $I = 10^{14} - 10^{16} \text{ W/cm}^2$.

This paper has a following outline: in Section 2 is shortly described tunneling ADK ionization rate in its corrected form, obtained by including Coulomb interaction in process of calculating turning point and taking into account the non-zero initial momentum of ejected electron. Section 3 is devoted to the discussion of gained results, while Section 4 contains a brief conclusion.

2. THEORETICAL BACKGROUND

In Ammosov, Delone and Krainov's paper [6] the expression for tunneling ADK ionization rate was given as

$$w_{\text{ADK}} = \left(\frac{3e}{\pi} \right)^{3/2} \left(\frac{16eE_i^2}{ZF} \right)^{2n^*-3/2} \frac{Z^2}{n^{9/2}} e^{-\frac{2Z^3}{3Fn^{*3}}}, \quad (1)$$

where Z is the nuclear charge of the ion residue of a given atom, while n^* is the effective principal quantum number given by expression $n^* = Z / \sqrt{2E_i}$.

As already noted, Coulomb interaction has been included in all aspects of the developing ADK theory except when turning point was calculated, and that oversight was corrected in paper [20]. In all calculations mentioned before it was also always assumed that ionized electron leaves the atom with zero initial momentum. If that is not the case, the corrected form of ionization rate must include the non-zero initial momentum as derived in [13, 14]

$$W_{if} = \left[\frac{4eZ^3}{Fn^{*4}} \frac{1}{1 + \frac{2ZF}{(p^2 + 2E_i)^2} + \frac{Z^2F^2}{(p^2 + 2E_i)^3 2E_i}} \right]^{2n^*-1} e^{-\frac{2Z^3}{3Fn^{*3}} - \frac{p^2\gamma^3}{3\omega}}. \quad (2)$$

In order to obtain the analytical expression for the non-zero initial momentum of the ejected electron the most suitable is to use parabolic coordinates: $\zeta = r + z$, $\eta = r - z$, $\phi = \arctan(y/x)$, where $\zeta, \eta \in [0, \infty)$ and ϕ is azimuthal angle whose values lie in the interval $[0, 2\pi]$ [21].

When the atom is placed in a linearly polarized laser field, ionization occurs along the η parabolic coordinate. Non-zero initial momentum of ejected electron is very sensitive to the laser electric field strength and to the position of the tunneling exit point, that is determined by expression $\eta_{\text{exit}} \cong 1/F$ and lies within range $1 \ll \eta \ll \eta_{\text{exit}}$ [21, 22].

Now, non-zero momentum p can be represented in two ways: in its exact form based on work by Bisgaard-Madsen [23]

$$p^{\text{BM}} = \sqrt{-\left(\frac{\kappa}{2}\right)^2 + \frac{\beta_2}{\eta} - \frac{m_l^2 - 1}{4\eta} + \frac{F\eta}{4}}, \quad (3)$$

where $\kappa = \sqrt{2E_i}$, $\beta_2 = Z - \frac{\kappa}{2}(|m_l| + 1)$, and m_l is the magnetic quantum number;

Eq. (3) is valid in the range $\frac{\beta_2}{\kappa^2} \ll \eta \ll \frac{\kappa^2}{2}$, inside the barrier $\eta < \eta_0$ where $\eta_0 \approx \kappa^2/F$.

Another form for non-zero initial momentum was obtained by Bauer; he expanded Eq. (3) in Taylor series with a goal to obtain explicit expression for non-zero initial momentum inside and outside the barrier, depending on the values of η coordinate. In our research we retained the expression for this momentum outside the barrier [22]

$$p^{\text{Bauer}} = \frac{1}{2} \left(\sqrt{F\eta - 1} + \frac{1}{\eta\sqrt{F\eta - 1}} \right). \quad (4)$$

Ionization rate has been calculated using both formulas for non-zero initial momentum because we intended to determine the intensity range in which one of these formulas is dominant while influence of another one is negligible. Besides, we also wanted to compare how the spatial linear and LG(0,1)* distribution of various types of lasers (Ti:sapphire in near-infrared, 800 nm, and CO₂ in mid-infrared range, 10.6 μm, of wavelength spectrum) affects the physical quantities of interest [24].

When the laser field is linearly polarized (non-phased), its strength is given by the following formula

$$F = \frac{27.5}{5.1 \times 10^9} \sqrt{I}, \quad (5)$$

where I is the intensity of the laser field being used, while the coefficient before square root stems from conversion to atomic unit system. On other hand, the strength of radially polarized laser field with LG(0,1)* spiral phase mode field distribution after being passed through linear polarizer can be expressed as [18, 25]

$$F_{\text{spiral}} = F \sqrt{\frac{2a^2 e^{2k\varphi}}{R^2}} e^{-\frac{a^2 e^{2k\varphi}}{R^2}} \cos \varphi, \quad (6)$$

where R is beam diameter, a is dimensionless parameter, $k = \tan \theta$, θ is the angle that determines a spiral geometry of the laser beam, while φ is azimuthal angle measured from the x -axis and lie in an interval span of $[0, 2\pi]$.

3. RESULTS AND DISCUSSION

In the discussion of obtained results, we first dealt with tunneling ionization rates, depending on various form of non-zero initial momentum of ejected electron; then we analyzed how ionization rate is influenced by different laser types and pulse shapes (compared for two ionization rate forms). Also, review of ionization rates values for alkali atoms is given. For each part corresponding graphs and an elaborate discussion is presented.

Our study is based on two laser systems, the Ti:sapphire laser system with following parameters: wavelength $\lambda_{\text{Ti:sapp}} = 800 \text{ nm}$ and photon energy $\omega_{\text{Ti:sapp}} = 0.0570 \text{ a.u.}$, and CO₂ laser system whose parameters are: wavelength $\lambda_{\text{CO}_2} = 10.6 \mu\text{m}$ and photon energy $\omega_{\text{CO}_2} = 0.0043 \text{ a.u.}$ It is important to emphasize that linearly polarized laser beam has a diameter that ranges widely (from μm even to mm), while radially polarized beam is very focused (order of a micrometer). In this research beam diameter R is fixed at the value of $3 \mu\text{m}$ ($5.7 \times 10^4 \text{ a.u.}$) [26, 27]. When beam dimensions are the order of μm , the dimensionless parameter is $a = 0.57$ ($1.08 \times 10^{14} \text{ a.u.}$). The constant k is calculated using the expression $k = \tan \theta$ (where the values for θ lie in the interval $[-\pi/2, \pi/2]$) and it determines the spiral geometry of the beam [25].

The alkali metals whose tunneling ionization process we analyzed have the ionization potentials (in atomic units): $E_i(\text{Li}) = 0.1981$, $E_i(\text{Na}) = 0.1888$, $E_i(\text{K}) = 0.1595$, $E_i(\text{Rb}) = 0.1535$, $E_i(\text{Cs}) = 0.1431$, $E_i(\text{Fr}) = 0.1447$. In these calculations the values of quantum numbers used are $n = 1$ and $m_l = 0$, while the charge of an ionized atom is $Z = 1$. Taking all into account, in figures below the results for Li and Fr atoms are presented (because they are the first and the last alkali group element), while detailed values of interest are given for all alkali atoms in Appendix. At the same place are given the calculated values for tunneling distance $d_{\text{exit}} = E_i/F$ in order to illustrate the additional differences between ionization process when dissimilar types of lasers are used, and also the influence of different laser beam profiles [28].

The influence of both linear and spiral-phase mode on non-zero initial momentum for Li atom as a typical representative of alkali metal group is given in Fig. 2. It is obvious that the values for momentum are diminished for spiral-phase scenario as compared to the linear. The other alkali metals are not shown since results obtained for them are very similar.

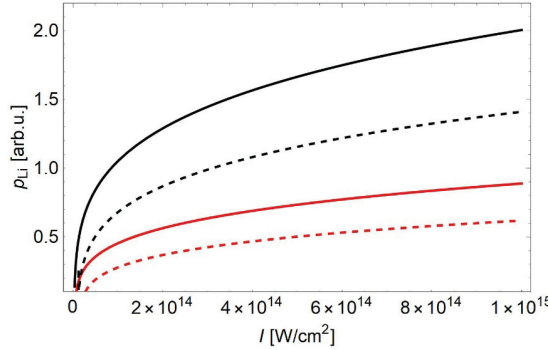


Fig. 2 – (Color online) Non-zero initial momentum of ejected valence electron of Li atom dependent on laser intensity: $p_{\text{Bauer}}^{\text{Bauer}}$ (black, solid line), $p_{\text{spiral}}^{\text{Bauer}}$ (black, dashed line), $p_{\text{Bauer}}^{\text{BM}}$ (red, solid line), $p_{\text{spiral}}^{\text{BM}}$ (red, dashed line).

The top graph row in Fig. 3 shows that ionization rate in the case of non-phased linearly polarized laser beam, while dependent on various expressions for non-zero initial momentum, is sensitive to the type of laser used for intensities below 10^{15} W/cm 2 . The bottom row of graphs shows that, at the higher intensities, the ionization rate is not sensitive on the aforementioned anymore.

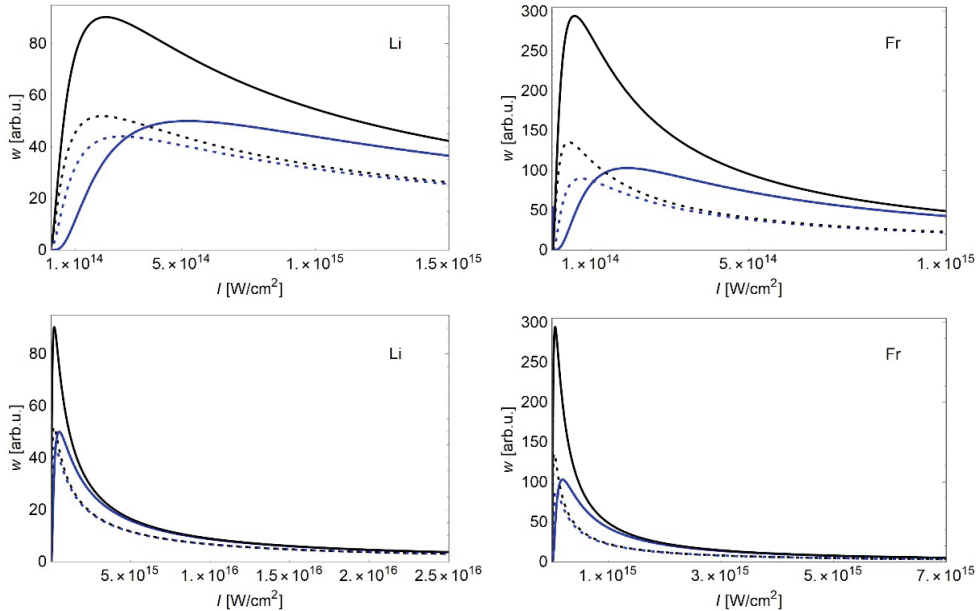


Fig. 3 – (Color online) Ionization rates of Li and Fr atoms for non-phased linearly polarized CO₂ laser: $w_{\text{Bauer}}^{\text{Bauer}}$ (black solid line), $w_{\text{Bauer}}^{\text{BM}}$ (black dotted line), and Ti:sapphire laser: $w_{\text{Bauer}}^{\text{Ti:sapphire}}$ (blue solid line), $w_{\text{Bauer}}^{\text{BM}}$ (blue dotted line).

It is interesting to note that in the case of Ti:sapphire laser the ionization rate lines for different expressions of non-zero initial momentum intersect: for Li, it happens at intensity value of $2.95 \times 10^{14} \text{ W/cm}^2$, while for Fr it is $1.07 \times 10^{14} \text{ W/cm}^2$.

All that was said for Fig. 3 is also valid for Fig. 4, although Fig. 4 shows the ionization rate for LG(0,1)* spiral-phased linearly polarized laser beam. Intensity ranges were adapted appropriately in order to make noticeable the decreasing slopes of the curves depicted. Same as above, in the case of Ti:sapphire laser the ionization rate lines intersect for different expressions of non-zero initial momentum, but on higher intensity values than those for non-phased linearly polarized laser beams: for Li, it now happens at intensity value of $1.085 \times 10^{15} \text{ W/cm}^2$, while for Fr the value is $3.88 \times 10^{14} \text{ W/cm}^2$.

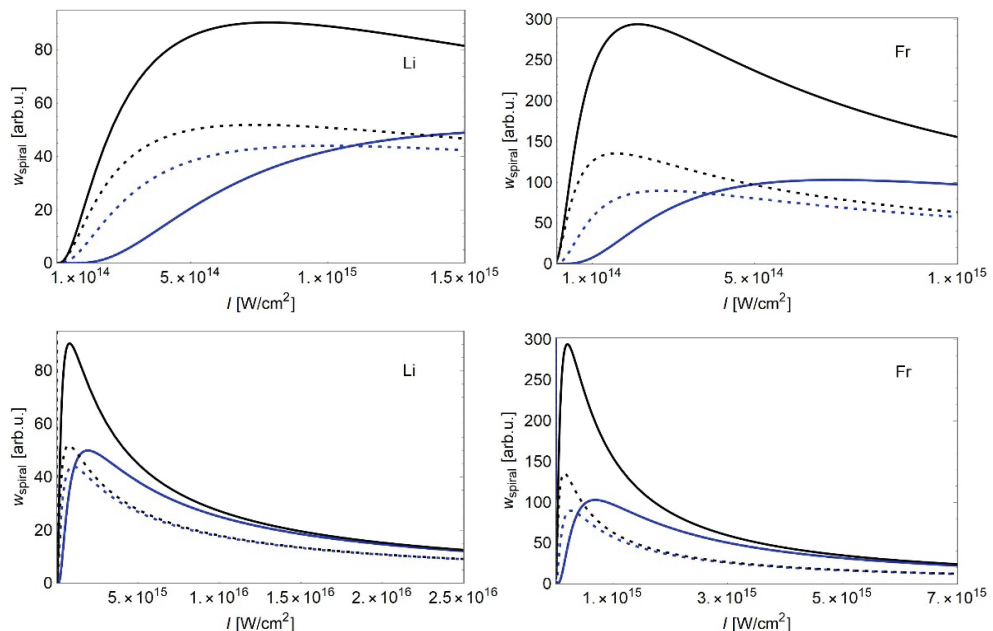


Fig. 4 – (Color online) Ionization rates of Li and Fr atoms for LG(0,1)* spiral-phased linearly polarized CO₂ laser: $w_{\text{spiral}}^{\text{Bauer}}$ (black solid line), $w_{\text{spiral}}^{\text{BM}}$ (black dotted line), and Ti:sapphire laser: $w_{\text{spiral}}^{\text{Bauer}}$ (blue solid line), $w_{\text{spiral}}^{\text{BM}}$ (blue dotted line).

Ionization rate that includes Bisgaard-Madsen formula has similar dependence for frequencies of both lasers in the case of non-phased linearly polarized and spiral-phased linearly polarized field distribution. Since Bauer formula for non-zero initial momentum is the first approximation of Bisgaard-Madsen formula, its usage shows that the ionization rate for both atoms in this case is more influenced by laser frequency.

However, comparing the ionization rates of both atoms in the case of non-phase linear polarization shows that their maxima are different: for Li, maximum appears at intensity of $2.15 \times 10^{14} \text{ W/cm}^2$ for p^{Bauer} and CO₂ laser; at intensity of $2.03 \times 10^{14} \text{ W/cm}^2$ for p^{BM} and CO₂ laser; at intensity of $5.23 \times 10^{14} \text{ W/cm}^2$ for p^{Bauer} and Ti:sapphire laser; at intensity of $2.74 \times 10^{14} \text{ W/cm}^2$ for p^{BM} and Ti:sapphire laser. For Fr atom, maximum appears at intensity of $5.82 \times 10^{13} \text{ W/cm}^2$ for p^{Bauer} and CO₂ laser; at intensity of $4.35 \times 10^{13} \text{ W/cm}^2$ for p^{BM} and CO₂ laser; at intensity of $1.91 \times 10^{14} \text{ W/cm}^2$ for p^{Bauer} and Ti:sapphire laser; at intensity of $7.52 \times 10^{13} \text{ W/cm}^2$ for p^{BM} and Ti:sapphire laser (Fig. 3).

Now, regarding the ionization rates of both atoms in the case of spiral-phase linear field distribution, the data are as follows: for Li, maximum appears at intensity of $7.85 \times 10^{14} \text{ W/cm}^2$ for $p_{\text{spiral}}^{\text{Bauer}}$ and CO₂ laser; at intensity of $7.39 \times 10^{14} \text{ W/cm}^2$ for $p_{\text{spiral}}^{\text{BM}}$ and CO₂ laser; at intensity of $1.91 \times 10^{15} \text{ W/cm}^2$ for $p_{\text{spiral}}^{\text{Bauer}}$ and Ti:sapphire laser; at intensity of $1.00 \times 10^{15} \text{ W/cm}^2$ for $p_{\text{spiral}}^{\text{BM}}$ and Ti:sapphire laser. For Fr atom, maximum appears at intensity of $2.12 \times 10^{14} \text{ W/cm}^2$ for $p_{\text{spiral}}^{\text{Bauer}}$ and CO₂ laser; at intensity of $1.58 \times 10^{14} \text{ W/cm}^2$ for $p_{\text{spiral}}^{\text{BM}}$ and CO₂ laser; at intensity of $6.96 \times 10^{14} \text{ W/cm}^2$ for $p_{\text{spiral}}^{\text{Bauer}}$ and Ti:sapphire laser; at intensity of $2.74 \times 10^{14} \text{ W/cm}^2$ for $p_{\text{spiral}}^{\text{BM}}$ and Ti:sapphire laser (Fig. 4).

At Fig. 5 is given the behavior of ionization rate depending on the laser intensity I , but also on photon energy ω for wavelengths within the broadened infrared range; this was made possible by recent developments in laser technology that extended strong field studies from near-infrared to the mid-infrared wavelength values. It is obvious that surfaces that represent the ionization rates w and w_{spiral} are intersecting with one another.

From 3D part of Fig. 5 can be easily ascertained that w^{BM} reaches its maximum at lower field intensities and is more dependent on laser frequency compared with $w_{\text{spiral}}^{\text{BM}}$, which is more stable.

The formula for laser intensity (obtained by fitting) on which the ionization rates w^{BM} and $w_{\text{spiral}}^{\text{BM}}$ have the same values is given as

$$I = -2.656 \times 10^{16} \omega^2 - 5.5 \times 10^{14} \omega^{1.5} + 4.4 \times 10^{14}, \quad (7)$$

depending on photon energy ω in the interval [0.00005, 0.06509] a.u. of infrared spectrum; that was shown at 3D part of Fig. 5.

The intersection curves given at 2D part of Fig. 5 confirm that the result is similar when momentum p^{Bauer} is included; in this case, the laser intensity formula

(for equal values of ionization rates w^{Bauer} and $w_{\text{spiral}}^{\text{Bauer}}$, also obtained by fitting, has the following form

$$I = -7.59 \times 10^{16} \omega^2 + 1.65 \times 10^{15} \omega^{1.1} + 4.1 \times 10^{14}, \quad (8)$$

for the same interval of the photon energy ω as above.

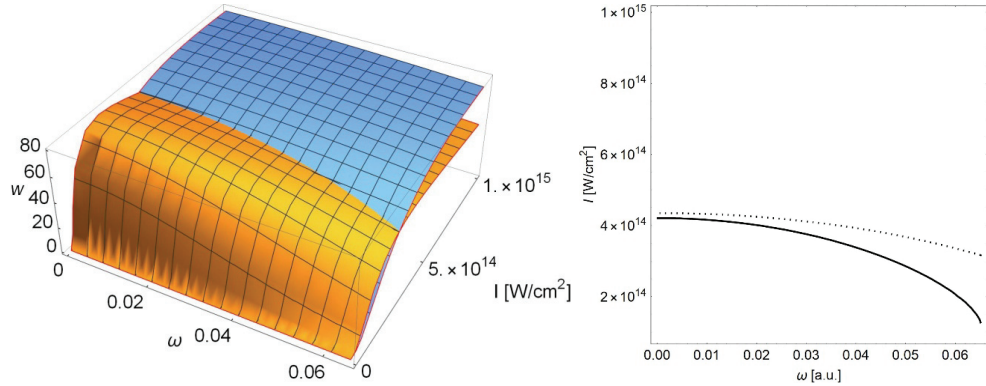


Fig. 5 – (Color online) Ionization rates w and w_{spiral} of Li, with non-zero initial momentum included, dependent on laser intensity and photon energy: a) orange-hued surface represents w^{BM} while blue-hued surface represents $w_{\text{spiral}}^{\text{BM}}$; b) solid curve represents intersection of w^{Bauer} and $w_{\text{spiral}}^{\text{Bauer}}$ surfaces, while dotted curve represents the same for w^{BM} and $w_{\text{spiral}}^{\text{BM}}$ surfaces.

However, for Fr atom, and for the same set of parameters, the ionization by spiral-phase linearly polarized laser field is more dominant than ionization by non-phase linearly polarized field. Differently than in the case of Li, where ionization is possible in the whole range of infrared frequencies, in the case of Fr, the ionization happens at smaller values and approximately ends at 0.04 a.u. (or $\lambda = 1.139 \mu\text{m}$).

In this case, the fitting formula for laser intensity on which the ionization rates w and w_{spiral} have the same values is given as

$$I = -10^{16.145} \omega^2 + 10^{11.3} (\omega - 3) + 1.1 \times 10^{14}, \quad (9)$$

with p^{Bauer} included, while when p^{BM} is included (3D part of Fig. 6), the formula is given as

$$I = -10^{16.42} \omega^2 + 12 \times 10^{10} (\omega + 3) + 1.132 \times 10^{14}, \quad (10)$$

for the interval of photon energy $[0.00005, 0.04]$ a.u. of infrared spectrum.

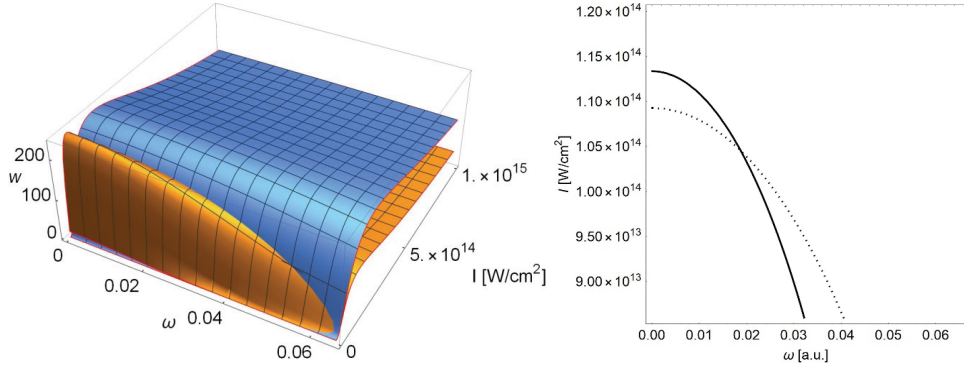


Fig. 6 – (Color online) Ionization rates w and w_{spiral} of Fr, with non-zero initial momentum included, dependent on laser intensity and photon energy: a) orange-hued surface represents w^{BM} while blue-hued surface represents $w_{\text{spiral}}^{\text{BM}}$; b) solid curve represents intersection of w^{Bauer} and $w_{\text{spiral}}^{\text{Bauer}}$ surfaces, while dotted curve represents the same for w^{BM} and $w_{\text{spiral}}^{\text{BM}}$ surfaces.

From 2D part of Fig. 6 is obvious that the values for ionization rates are the same regardless of polarization type along these intersection lines.

4. CONCLUSION

In the discussion of obtained results, we first dealt with tunneling ionization rates, depending on various form of non-zero initial momentum of ejected electron; then we analyzed how ionization rate is influenced by different laser types and pulse shapes (compared for two ionization rate forms). Also, review of ionization rates values for alkali atoms is given. For each part corresponding graphs and an elaborate discussion is presented.

In this paper the phenomenon of one electron tunneling through the potential barrier of alkali atoms deformed by laser field potential has been investigated. Our ionization rate analysis included the following: 1) the influence of Coulomb interaction on turning point of ADK theory; 2) the influence of the two forms of non-zero initial momentum of ejected electron, Bauer's, and Bisgaard-Madsen's; 3) the influence of two types of laser beam profiles, non-phased and spiral-phased.

Results of presented analysis will be given here: regardless of type of laser used or their frequencies, ionization rate with non-zero Bisgaard-Madsen momentum included exhibits the similar behavior in the intensity range $[10^{14}, 10^{16}] \text{ W/cm}^2$. However, with Bauer approximate formula included, ionization rate is noticeably more influenced by laser frequency and depends on phase-state of laser field distribution: non-phase and $\text{LG}(0,1)^*$ spiral-phase. According to previous remarks, we expect that the here considered laser field distributions will have appreciable influence on the yield of ions produced in tunneling process.

Appendix

Table 1
Ionization rates for various field intensities

	I	10^{12}	10^{13}	10^{14}	10^{15}
		Li			
w^{BM}	CO_2	1.36×10^{-8}	0.87	45.32	32.81
w^{Bauer}		2.53×10^{-8}	1.01	75.33	54.59
$w_{\text{spiral}}^{\text{BM}}$		8.37×10^{-19}	5.82×10^{-4}	15.64	78.52
$w_{\text{spiral}}^{\text{Bauer}}$		3.55×10^{-15}	6.11×10^{-4}	17.19	88.91
w^{BM}		5.88×10^{-19}	0.28	31.89	31.44
w^{Bauer}		2.01×10^{-17}	5.52×10^{-5}	11.42	43.99
$w_{\text{spiral}}^{\text{BM}}$		1.66×10^{-18}	2.82×10^{-8}	6.64×10^{-1}	53.25
$w_{\text{spiral}}^{\text{Bauer}}$		4.63×10^{-17}	2.40×10^{-7}	7.1×10^{-2}	42.99
		Na			
w^{BM}	CO_2	1.34×10^{-7}	1.90	56.04	32.59
w^{Bauer}		2.40×10^{-7}	2.23	97.58	56.11
$w_{\text{spiral}}^{\text{BM}}$		3.82×10^{-17}	2.50×10^{-3}	25.49	89.36
$w_{\text{spiral}}^{\text{Bauer}}$		1.17×10^{-13}	2.59×10^{-3}	28.29	101.99
w^{BM}		2.32×10^{-15}	5.09×10^{-1}	40.1	31.31
w^{Bauer}		3.82×10^{-19}	2.43×10^{-4}	16.87	45.83
$w_{\text{spiral}}^{\text{BM}}$		6.47×10^{-20}	4.50×10^{-8}	1.24	62.16
$w_{\text{spiral}}^{\text{Bauer}}$		2.56×10^{-17}	5.72×10^{-3}	1.71×10^{-1}	50.83
		K			
w^{BM}	CO_2	1.34×10^{-4}	18.54	95.54	27.67
w^{Bauer}		1.94×10^{-4}	23.99	200.84	54.50
$w_{\text{spiral}}^{\text{BM}}$		4.85×10^{-12}	2.01×10^{-1}	106.30	120.97
$w_{\text{spiral}}^{\text{Bauer}}$		3.79×10^{-9}	1.90×10^{-1}	122.39	142.39
w^{BM}		7.32×10^{-5}	3.59	72.23	26.81
w^{Bauer}		2.87×10^{-5}	2.01×10^{-2}	51.39	46.58
$w_{\text{spiral}}^{\text{BM}}$		5.88×10^{-10}	6.74×10^{-7}	8.95	90.88
$w_{\text{spiral}}^{\text{Bauer}}$		2.10×10^{-6}	7.53×10^{-1}	2.32	82.92

		Rb					
		CO ₂	5.18×10 ⁻⁴	28.54	103.13	25.84	
w^{BM}			6.99×10 ⁻⁴	37.82	227.67	52.67	
w^{Bauer}			5.05×10 ⁻¹¹	4.72×10 ⁻¹	138.81	125.46	
$w_{\text{spiral}}^{\text{BM}}$			2.75×10 ⁻⁸	4.35×10 ⁻¹	161.27	148.824	
		Ti:sapphire	2.04×10 ⁻⁴	5.37	78.89	25.08	
w^{BM}			5.09×10 ⁻⁵	4.70×10 ⁻²	62.87	45.41	
w^{Bauer}			3.64×10 ⁻⁸	1.44×10 ⁻⁶	13.08	95.71	
$w_{\text{spiral}}^{\text{BM}}$			5.68×10 ⁻⁷	1.23×10 ⁻²	3.81	89.32	
Cs							
		CO ₂	5.16×10 ⁻³	58.14	113.72	22.12	
w^{BM}			5.87×10 ⁻³	80.75	276.28	48.15	
w^{Bauer}			2.77×10 ⁻⁹	2.00	214.73	130.04	
$w_{\text{spiral}}^{\text{BM}}$			7.21×10 ⁻⁷	1.73	253.84	156.54	
		Ti:sapphire	1.15×10 ⁻³	10.70	88.82	21.52	
w^{BM}			1.13×10 ⁻⁴	1.96×10 ⁻¹	86.75	42.13	
w^{Bauer}			5.11×10 ⁻¹⁰	6.25×10 ⁻⁶	24.63	101.79	
$w_{\text{spiral}}^{\text{BM}}$			5.14×10 ⁻⁵	2.78×10 ⁻²	8.73	98.87	
Fr							
		CO ₂	3.64×10 ⁻³	52.28	112.38	22.73	
w^{BM}			4.27×10 ⁻³	72.05	268.76	48.95	
w^{Bauer}			1.50×10 ⁻⁷	1.61	201.26	129.65	
$w_{\text{spiral}}^{\text{BM}}$			4.43×10 ⁻⁷	1.40	237.25	155.70	
		Ti:sapphire	2.32×10 ⁻³	9.64	87.49	22.11	
w^{BM}			5.74×10 ⁻⁴	1.58×10 ⁻¹	82.76	42.74	
w^{Bauer}			1.86×10 ⁻¹⁰	4.93×10 ⁻⁶	22.40	101.09	
$w_{\text{spiral}}^{\text{BM}}$			6.52×10 ⁻¹⁰	2.46×10 ⁻²	7.71	97.58	

Table 2

Numerical values of maximal ionization rate, in non-phased and spiral-phased case, with Bauer and BM momentum included, for all alkali elements

CO₂						
	I [10 ¹⁴ W cm ⁻²]	w^{BM} [a.u.]	d_{exit} [a.u.]	I [10 ¹⁴ W cm ⁻²]	w^{Bauer} [a.u.]	d_{exit} [a.u.]
Li	2.03	51.89	2.58	2.12	91.16	2.52
Na	1.70	59.46	2.69	1.75	107.47	2.65
K	0.70	98.85	3.54	0.86	202.18	3.19
Rb	0.58	101.70	3.74	0.74	234.22	3.31
Cs	0.41	140.76	4.13	0.56	307.08	3.55
Fr	0.43	135.60	4.09	0.58	294.16	3.51
	I [10 ¹⁴ W cm ⁻²]	$w^{\text{BM}}_{\text{spiral}}$ [a.u.]	d_{exit} [a.u.]	I [10 ¹⁴ W cm ⁻²]	$w^{\text{Bauer}}_{\text{spiral}}$ [a.u.]	d_{exit} [a.u.]
Li	8.05	79.41	1.29	7.85	90.28	1.31
Na	6.55	93.43	1.37	6.37	107.47	1.39
K	3.12	168.49	1.67	3.15	202.18	1.67
Rb	2.64	193.46	1.75	2.69	234.22	1.74
Cs	1.94	250.11	1.91	2.03	307.09	1.86
Fr	2.05	240.05	1.87	2.12	294.16	1.84

Ti:sapphire

	I [10 ¹⁴ W cm ⁻²]	w^{BM} [a.u.]	d_{exit} [a.u.]	I [10 ¹⁵ W cm ⁻²]	w^{Bauer} [a.u.]	d_{exit} [a.u.]
Li	2.75	44.02	2.22	0.53	50.0	1.60
Na	2.24	49.24	2.34	0.44	56.08	1.67
K	1.11	72.48	2.81	0.26	89.03	1.83
Rb	0.95	78.96	2.92	0.23	90.50	1.88
Cs	0.72	92.07	3.13	0.18	105.58	1.95
Fr	0.75	89.88	3.1	0.19	103.07	1.94

	I [10 ¹⁵ W cm ⁻²]	$w^{\text{BM}}_{\text{spiral}}$ [a.u.]	d_{exit} [a.u.]	I [10 ¹⁵ W cm ⁻²]	$w^{\text{Bauer}}_{\text{spiral}}$ [a.u.]	d_{exit} [a.u.]
Li	1.40	55.84	0.98	1.91	50.00	0.84
Na	1.20	63.06	1.01	1.63	56.10	0.87
K	0.70	95.16	0.72	0.95	83.03	0.96
Rb	0.62	104.04	1.14	0.83	90.50	0.99
Cs	0.50	121.83	1.19	0.67	105.58	1.03
Fr	0.51	118.89	1.19	0.70	103.06	1.01

Acknowledgements. The authors acknowledge funding provided by the University of Kragujevac – Institute for Information Technologies (the contract 451-03-9/2021-14/200378), University of Kragujevac – Faculty of Science (the contract 451-03-9/2021-14/200122) through the grants by the Ministry of Education, Science and Technological Development of the Republic of Serbia.

REFERENCES

1. N. I. Shvetsov-Shilovski, M. Lein and K. Tőkési, Eur. Phys. J. D **73**, 37 (2019).
2. Yuan Minghu, Opt. Express **27**, 6502–6511 (2019).
3. Jakub S. Prauzner-Bechcicki, Dmitry K. Efimov, Michał Mandrysz and Jakub Zakrzewski, J. Phys. B: At. Mol. Opt. Phys. **54** (11), 114001 (2021).
4. L.V. Keldysh, Soviet Physics JETP **20**, 1307–1314 (1965).
5. A.M. Perelomov, V.S. Popov and M.V. Terent'ev, Soviet Physics JETP **23**, 924–934 (1966).
6. M.V. Ammosov, N.B. Delone and V.P. Krainov, Soviet Physics JETP **64**, 1191–1194 (1986).
7. Yu Hung Lai *et al.*, Phys. Rev. A **96**, 063417 (2017).
8. N.B. Delone and V.P. Krainov, *Multiphoton Processes in Atoms*, Springer-Verlag, Berlin, Heidelberg, 1994.
9. Chuan Liang Wang *et al.*, Phys. Rev. A **90**, 013422 (2014).
10. Yang Li *et al.*, Opt. Express **23**, 28801–28807 (2015).
11. Minghu Yuan *et al.*, Optics Express, **25**, 19, 23493–23501 (2017).
12. Jun Cai *et al.*, Phys. Rev. A **96**, 033413 (2017).
13. V.P. Krainov and V.M. Ristić, Sov. Phys. JETP **74**(5), (1992).
14. V.M. Ristić, T.B. Miladinović and M.M. Radulović, Acta Phys. Pol. A, **112** (5), 909–914 (2007).
15. V.M. Ristić, T.B. Miladinović and M.M. Radulović, Acta Phys. Pol. A, **116** (4), 504–506 (2009).
16. C. Maurer, A. Jesacher, S. Fürhapter, S. Bernet and M. Ritsch-Marte, New J. Phys. **9**, 78 (2007).
17. R. Oron, N. Davidson, A. Friesem and E. Hasman, Opt. Lett. **25**, 939–941 (2000).
18. G. Machavariani *et al.*, *Effect of the spiral phase element on the radial-polarization (0, 1)*LG beam*, Optics Communications, **271** (1), 190–196 (2007).
19. A. Tovar, J. Opt. Soc. Am. A, **15** (10), 2705–2711 (1998).
20. V. M. Ristić, M. M. Radulović and V.P. Krainov, Laser Physics **4**, 928–932 (1998).
21. L. D. Landau and E. M. Lifshitz, *Course of Theoretical Physics*, Vol. 3: *Quantum Mechanics: Non-Relativistic Theory*, Pergamon Press, Oxford, 1991.
22. D. Bauer, *Theory of Laser-Matter Interaction*, Max-Planck-Institut für Kernphysik, Heidelberg, 2006.
23. C. Z. Bisgaard and L. B. Madsen, Am. J. Phys. **72** (2), 249–254 (2004).
24. Dunzhao Wei *et al.*, Phys. Rev. Applied **11**, 014038 (2019).
25. J. Ouyang *et al.*, Opt. Express **23**, 12562 (2015).
26. R. Dorn, S. Quabis, and G. Leuchs, Phys. Rev. Lett. **91**, 233901 (2003).
27. K. M. Tanvir Ahmed, C. Grambow and A. M. Kietzig, Micromachines **5**(4), 1219 (2014)
28. S. L. Chin, *Advances in multi-photon processes and spectroscopy*, **16**, World Scientific, 2004.